Improved Mass Detection in 3D Automated Breast Ultrasound Using Region Based Features and Multi-view Information

Chuyang Ye[1], Vivek Vaidya[2], and Fei Zhao[3]

***Abstract*— Breast cancer is one of the leading causes of cancer death for women. Early detection of breast cancer is crucial for reducing mortality rates and improving prognosis of patients. Recently, 3D automated breast ultrasound (ABUS) has gained increasing attentions for reducing subjectivity, operator-dependence, and providing 3D context of the whole breast. In this work, we propose a breast mass detection algorithm improving voxel-based detection results by incorporating 3D region-based features and multi-view information in 3D ABUS images. Based on the candidate mass regions produced by voxel-based method, our proposed approach further improves the detection results with three major steps: 1) 3D mass segmentation in geodesic active contours framework with edge points obtained from directional searching; 2) region-based single-view and multi-view feature extraction; 3) support vector machine (SVM) classification to discriminate candidate regions as breast masses or normal background tissues. 22 patients including 51 3D ABUS volumes with 44 breast masses were used for evaluation. The proposed approach reached sensitivities of 95%, 90%, and 70% with averaged 4.3, 3.8, and 1.6 false positives per volume, respectively. The results also indicate that the multi-view information plays an important role in false positive reduction in 3D breast mass detection.**

***Index Terms*— ABUS, breast cancer, multi-view, geodesic active contours, SVM**

I. INTRODUCTION

Breast cancer is the second leading cause of cancer death for the women in the United States [1]. Early detection is important for better treatment to reduce the death rate. Ultrasound imaging has been used as an adjunct to mammography, serving as a screening tool to detect breast masses, and has gradually gained popularity. Compared to mammography, ultrasound imaging is less expensive, more sensitive for detecting abnormalities in dense breasts, and introduces no radiation. Since the manual mass detection on ultrasound images can be time-consuming and subjective, Computer-aided detection (CAD) of breast masses has been explored by researchers. The goal of the CAD system is to achieve high sensitivities and maintain low false positive rates. A standard breast mass CAD system includes a pre-processing step, a mass candidate segmentation step, and a classification step [2]. The pre-processing step reduces noise and artifacts of input images. Then mass candidates are segmented with different methods, such as thresholding [3], active contours [4], and Markov random field [5]. From the segmented regions of interest (ROIs), features that represent texture, morphology, and appearance can be extracted and fed into classifiers, such as neural network [6] and support vector machine (SVM) [4], to determine if a candidate is a true mass or normal background tissue.

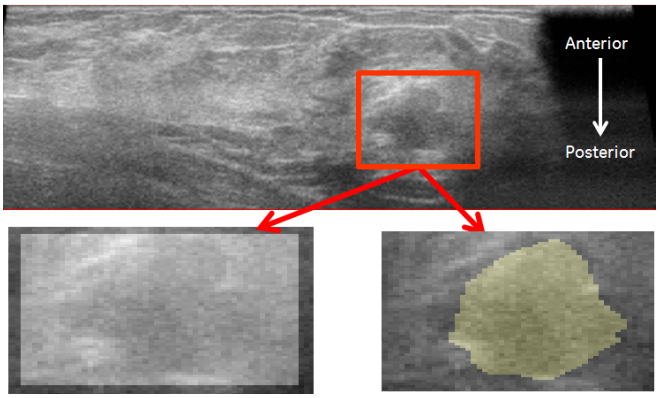

Fig. 1. An example of breast mass on ultrasound images. Top: a breast mass overlaid on the ultrasound image on a representative slice. Bottom left: zoom-in view with a bounding mask (white) labeled by doctors. Bottom right: zoom-in view with the segmentation (yellow) generated by the proposed method. Note the intensity inhomogeneity and weak boundaries.

Most of the existing works are developed based on 2D ultrasound images. In recent years, 3D automated breast ultrasound (ABUS) imaging has been proposed, which overcomes the disadvantages of operator dependency and limited view of breasts in 2D hand-held ultrasound imaging. Moon [7] and Tan [8] proposed 3D CAD following similar standard 2D CAD framework, where the classification follows the segmentation of candidate ROIs. In 3D ABUS, to completely scan the whole breast, two to five acquisitions are required in slightly different orientations. These scans yield multiple views of the same breast masses with large overlapping regions. Although 3D ABUS provides important multi-view information for breast masses, existing ABUS CADs assume these views are independent, and do not take this information into account.

In this work, we propose a 3D breast mass detection approach to improve our recently developed voxel level mass detection [9], by incorporating 3D region-based features. More important, we explore the multi-view dependencies to further reduce the false positives in 3D ABUS images. Based on the candidate mass regions produced by voxel level method, our proposed approach further improves the detection results with the following major steps. 1) Mass segmentation: In 3D ultrasound images, intensity inhomogeneity inside the masses and weak contrasts at mass edges can are well-known challenges for segmentation in ultra-

[1]Department of Electrical and Computer Engineering, Johns Hopkins University, Baltimore, MD, USA cye4@jhu.edu
[2]GE Global Research, Bangalore, 560066, India
[3]GE Global Research, Niskayuna, 12309, USA zhaof@ge.com

978-1-4244-7929-0/14/$26.00 ©2014 IEEE

sound images. Fig. 1 gives such an example. The mass boundary is strong at the anterior part, however, for some regions at the lateral and posterior boundaries, the edges start to fade; and inside the mass, image inhomogeneities are recognizable. The image quality increases the difficulties of segmentation and reliable extraction of features from segmented candidates, and thus mass detection is also influenced. To address this problem, the proposed method locates the candidate boundaries with a directional search of edge points. These edge points are further converted to boundary information which is used in the geodesic active contours for a robust segmentation. 2) Feature extraction: Region-based features including texture, shape, intensity, etc., are first extracted from segmentation regions. Since different views of the same subject are dependent, in addition to extracting region-based features from each candidate independently as previous works, we compute features by incorporating the multi-view information. For each candidate region, the multi-view features are computed by measuring its similarity to all other candidates across different views. This similarity measurement approach is based on the assumption that the same masses detected in multiple views share similar shape and appearance features, while false detections caused by noise and artifacts are less likely to appear in different views. 3) Classification: Features extracted from both single view and multiple views are fed into the SVM to discriminate each candidate region as a true mass or normal background tissue. Details of each step are given in the next section.

II. METHODS

A. Voxel-Based Candidate Generation

Recently, we developed a novel topological texture feature-based approach for mass detection in voxel level [9]. Concatenating with gradient concentration filter, this voxel-based approach extracts topological texture feature named Minkowski functional for each voxel and utilizes a classifier to label each voxel as a breast mass voxel or normal tissue voxel. The effectiveness of this mass detection approach has been justified on 2D breast ultrasound images. In this work we apply this 2D voxel-based approach along sagittal, coronal, and transverse views sequentially to produce 3D mass candidate regions. Detailed description of the voxel-based approach is beyond the scope of this paper and can be found in [9]. Although this voxel-based approach yields high sensitivity, there are two limitations: 1) due to the inhomogeneity and weak edges in 3D ABUS, the voxel-based approach doesn't generate accurate 3D representations of the masses; 2) there are relatively high false positive rates caused by artifacts and other normal tissues sharing similar texture properties as masses. We further improve this voxel-based detection results using a mass segmentation approach and classification based on region-based features and multi-view information.

B. Candidate Segmentation

To better extract reliable region-based features, a 3D geodesic active contours (GAC) [10] framework is used to produce more accurate mass candidate segmentation. Firstly, we smooth the input image using the method in [11] to suppress speckle noise. Then, using a level set function to represent the object, the GAC evolves the object boundary based on intensity information, as shown below:

$$\frac{\partial u}{\partial t} = g(I)|\nabla u|\kappa + \nabla g(I) \cdot \nabla u, \tag{1}$$

where u is the level set function, $g(\cdot)$ is a positive decreasing "edge detector" function, and I is the image intensity [10]. Here we choose $g(I)$ as:

$$g(I) = \frac{1}{1 + \exp\{\frac{|(\nabla * G)(I)| - \beta}{\alpha}\}}, \tag{2}$$

where $\nabla * G$ is the derivative of Gaussian operator, and α and β are constants.

However, due to inhomogeneity and weak edges, $|(\nabla * G)(I)|$ does not always detect true edges. Directly evolving the candidate regions on the intensity image fails because the segmentation can easily be trapped in local maxima. To tackle this challenge, a directional search of edge points is first applied. Specifically, from the center of the candidate seed regions, a set of rays in each direction are created, and the points within a range on each ray are inspected receptively. An illustration of the searching process is give in Fig. 2(a). Inside the candidate, all the points on the ray are considered; outside the initial candidate region, only points within a distance of r_{max} to the candidate boundary in the direction are considered. Among the points with increasing gradient, the one with the maximum gradient magnitude is selected as the edge point in this direction. The increasing gradient constraint is enforced because the mass has lower intensity than the regions outside. An example of the edge points is given in Fig. 2(b).

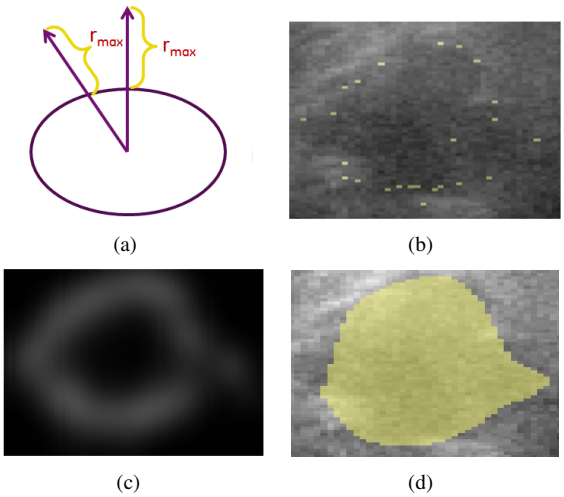

Fig. 2. Directional search of edges. (a) An illustration of directional searching process. (b) An example of edge points (yellow dots). (c) An example of edge maps generated from edge points. (d) Segmentation based on the edge map.

The edge points give the approximate locations of edges. To use them in the GAC, we calculate edge maps using

these points. A Gaussian blur is applied on the points. Dense edge points produce strong edges and sparse edge points give low intensities on the edge map. Also because the search of edge points is radial and points get sparser with larger radii, a compensation of the distance to the origin of the rays is made. The square of the distance to the ray origin is multiplied on the edge map. An example of the compensated edge map is shown in Fig. 2(c).

With the edge map, the GAC can be used to obtain the segmentation. A bounding box containing the edge point is used as an initialization. With $|(\nabla * G)(I)|$ in (2) replaced by the edge map, the GAC evolves the boundary of each candidate. The result is close to the edges on the intensity image, as shown in Fig. 2(d). Because the edge map is built from smoothing a set of edge points, some details in the intensity image are lost. Thus a final refinement is done by using this result as the initialization and running another GAC on the intensity image as in (1) to include the details.

C. Feature Extraction

1) Single-View Features: For each candidate segmentation region, single-view features are extracted from individual ABUS volumes independently. To capture shape features, the width, height, depth, and volume of the candidate are used as shape descriptors. To capture appearance features, the mean and the variance of the intensity in the mass are used as intensity features; the contrast, shade, energy, and entropy of the gray level co-occurrence matrix (GLCM) [12], and the Sobel operator are used for texture representation. Here we apply the Sobel operator in anterior-posterior direction and inferior-superior direction respectively. In each result image, the mean and the variance of the intensity inside the segmentation regions are computed as the Sobel operator features. To incorporate the information from mass background regions, posterior acoustic feature [13], mass boundary [13], normalized radial gradient (NRG) [3], and minimum side difference (MSD) [3] are also computed.

2) Multi-View Features: In our 3D ABUS data, more than two scans with slightly different orientations are performed to cover the whole breast. These scans have large overlapping regions, which increases the probability that a mass appears in more than volumes. The same masses detected in multiple views share similar shape and appearance features, while false detections caused by ultrasound artifacts are less likely to appear in different views. Therefore, feature similarity measurements across different views are computed as multi-view features. Given a single breast scanned in N different views, with M_i candidate masses detected in each single view i, we represent candidate masses in view i as $L_{i,1}, L_{i,2}, ..., L_{i,M_i}$. For any single-view feature $x(i,j)$ extracted from $L_{i,j}, j \in \{1,2,...,M_i\}$, we compare it with the corresponding feature $x(k,l)$ extracted from the candidates $L_{k,l}$ in other views ($k \neq i, k \in \{1,2,...,N\}, l \in \{1,2,...,M_k\}$), and the absolute difference $\Delta x(i,j,k,l) = |x(i,j) - x(k,l)|$ is computed. Then the minimum is used as the *multi-view* feature $x_{\mathrm{mv}}(i,j)$:

$$x_{\mathrm{mv}}(i,j) = \min_{\substack{k \neq i, \\ l \in \{1,2,...,M_k\}}} |x(i,j) - x(k,l)|. \quad (3)$$

Compared to false detection caused by artifacts, the true mass has higher probability of appearing on more than one views, thus the minimum similarity measurement for each feature is smaller for true mass candidates. A subset of the single-view features is selected for multi-view similarity measurement computation. Features that tend to share similar characteristics between true masses and false detections in different views, such as the mean intensity, are not selected. In this work, the GLCM entropy [12], the posterior acoustic feature [13], the lesion boundary [13], the Sobel operator features, and the distance between mass candidate to nipple are used for calculating multi-view features using (3).

D. Classification

Combining the single-view features and multi-view features, each candidate region is represented by a 33 dimensional feature vector. A non-linear SVM [14] classifier with radial basis kernel function is used for final mass discrimination. The implementation of LIBSVM [15] is used in this work.

III. EXPERIMENTS AND EVALUATIONS

The proposed approach was evaluated on 22 patients with 51 3D ABUS volumes. Each patient was scanned with more than one views. Images were obtained on a GE Somo•v ABUS system. 44 masses were manually labeled by a radiologist. Since our approach is developed to reduce radiologists' reading burden during screening, the focus is on mass (including benign and malignant) detection instead of mass characterization (diagnosis). The manually labeled ground truth is sufficient to validate our screening tool, and no biopsy reference was used in this experiment.

The voxel-based candidate generation steps reached 95% sensitivity with 6.3 false detections per volume on average. Therefore, overall 364 mass candidate regions, including true masses and false detections, were used as inputs to our segmentation and classification pipeline. Two cross-sectional examples of the segmentation results are shown in Fig. 3. The left column shows two original mass regions with bounding

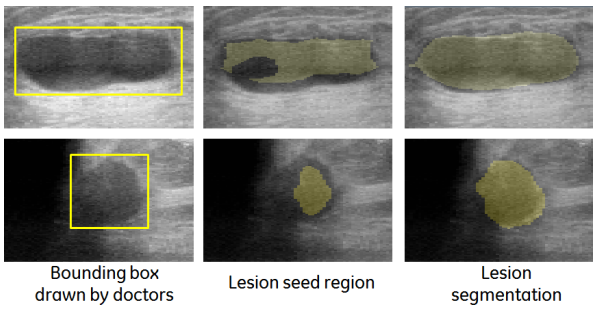

Fig. 3. Examples of lesion segmentation. Shown together with the bounding boxes representing the ground truth (labeled by radiologists) and the seed regions generated using voxel-based approach [9].

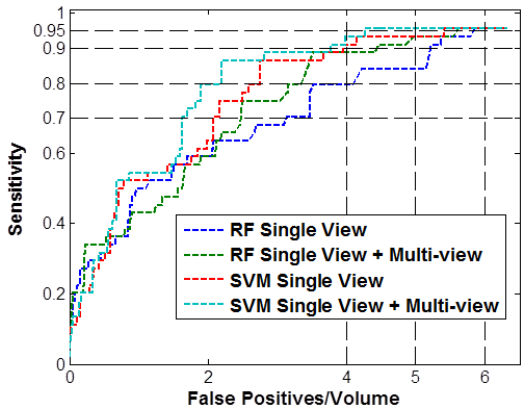

Fig. 4. FROCs of SVM and RF with and without multi-view features.

boxes of the ground truth labeled by radiologists. The seed regions generated using the voxel-based approach [9] are shown in the middle column. Lastly, the final segmentation results using our approach are shown in the right column. It can be seen that the proposed segmentation produces more complete and accurate segmentation results than the seed regions generated from the voxel-based approach. Also notice the large size differences between the two mass examples, where our approach yields good segmentations on masses with large size variation.

The final classification performance was evaluated using free response operating curve (FROC). Patient-based 11 fold cross-validation was used in the classification evaluation. To evaluate the performance of the SVM classifier, the random forest [16] classifier was also built for comparison. Standard parameters are used for the RF classifier. To evaluate the importance of using multi-view features for false detection reduction, classifiers using only single-view features and single-view plus multi-view features were built respectively and compared. The FROCs are plotted in Fig. 4. Three selected FROC operating points at sensitivities of 70%, 90% and 95% are shown in Table I. Overall, the SVM classifier performs better than the RF classifier in our task, with larger area under curve. For both classifiers, adding multi-view information improves detection by reducing false positives while maintaining the same sensitivity. Based on the voxel-level input with 6.3 false positives per volume, we reduce the averaged false positives to 5.4 with single-view region-based features, and then further reduce this number to 4.3 by incorporating multi-view features at sensitivity level as high as 95%. Slightly dropping the sensitivity to 90%, our approach reaches 3.7 false positives per volume, yielding over 40% false positive reduction.

IV. CONCLUSIONS

In this work, we proposed an improved 3D breast mass detection approach by combing both 3D region based features and multi-view features in ABUS images. Better 3D mass segmentation is produced by incorporating boundary information obtained from directional searching of edge points into the GAC framework. The shape and appearance

TABLE I

NUMBER OF FALSE POSITIVES PER VOLUME AT SENSITIVITY 70%, 90%, AND 95%. (SV=SINGLE VIEW, MV=MULTI-VIEW)

Sensitivity	RF SV	RF SV+MV	SVM SV	SVM SV+MV
70%	3.1	2.5	2.1	**1.6**
90%	5.2	4.5	3.9	**3.8**
95%	5.8	5.6	5.4	**4.3**

features extracted from segmentation regions are important for discriminating the true masses from false detections. The multi-view information plays an important role in false positive reduction during screening. The combination of both single-view and multi-view features reduced false detections dramatically while maintaining a high detection rate of 95% in 3D ABUS images.

REFERENCES

[1] J. Ma and A. Jemal, "Breast cancer statistics," in *Breast Cancer Metastasis and Drug Resistance*, A. Ahmad, Ed. Springer New York, 2013, pp. 1–18.

[2] H. Cheng, J. Shan, W. Ju, Y. Guo, and L. Zhang, "Automated breast cancer detection and classification using ultrasound images: A survey," *Pattern Recognition*, vol. 43, no. 1, pp. 299–317, 2010.

[3] K. Horsch, M. L. Giger, L. A. Venta, and C. J. Vyborny, "Computerized diagnosis of breast lesions on ultrasound," *Medical Physics*, vol. 29, p. 157, 2002.

[4] R.-F. Chang, W.-J. Wu, W. Moon, and D.-R. Chen, "Automatic ultrasound segmentation and morphology based diagnosis of solid breast tumors," *Breast Cancer Research and Treatment*, vol. 89, no. 2, pp. 179–185, 2005.

[5] G. Xiao, M. Brady, J. A. Noble, and Y. Zhang, "Segmentation of ultrasound B-mode images with intensity inhomogeneity correction," *Medical Imaging, IEEE Transactions on*, vol. 21, no. 1, pp. 48–57, 2002.

[6] C.-M. Chen, Y.-H. Chou, K.-C. Han, G.-S. Hung, C.-M. Tiu, H.-J. Chiou, and S.-Y. Chiou, "Breast lesions on sonograms: Computer-aided diagnosis with nearly setting-independent features and artificial neural networks," *Radiology*, vol. 226, no. 2, pp. 504–514, 2003.

[7] W. K. Moon, Y.-W. Shen, M. S. Bae, C.-S. Huang, J.-H. Chen, and R.-F. Chang, "Computer-aided tumor detection based on multi-scale blob detection algorithm in automated breast ultrasound images," *Medical Imaging, IEEE Transactions on*, vol. 32, no. 7, pp. 1191–1200, 2013.

[8] T. Tan, B. Platel, R. Mus, L. Tabar, R. Mann, and N. Karssemeijer, "Computer-aided detection of cancer in automated 3-D breast," *Medical Imaging, IEEE Transactions on*, vol. 32, no. 9, pp. 1698–1706, 2013.

[9] F. Zhao, X. Li, S. Biswas, R. Mullick, P. Mendonca, and V. Vaidya, "Topological texture-based method for mass detection in breast ultrasound image," in *accepted, ISBI*, 2014, pp. *–*.

[10] V. Caselles, R. Kimmel, and G. Sapiro, "Geodesic active contours," *International journal of computer vision*, vol. 22, no. 1, pp. 61–79, 1997.

[11] G. Slabaugh, G. Unal, M. Wels, T. Fang, and B. Rao, "Statistical region-based segmentation of ultrasound images," *Ultrasound in medicine & biology*, vol. 35, no. 5, pp. 781–795, 2009.

[12] R. M. Haralick, K. Shanmugam, and I. H. Dinstein, "Textural features for image classification," *Systems, Man and Cybernetics, IEEE Transactions on*, no. 6, pp. 610–621, 1973.

[13] W.-C. Shen, R.-F. Chang, W. K. Moon, Y.-H. Chou, and C.-S. Huang, "Breast ultrasound computer-aided diagnosis using BI-RADS features," *Academic radiology*, vol. 14, no. 8, pp. 928–939, 2007.

[14] C. Cortes and V. Vapnik, "Support-vector networks," *Machine learning*, vol. 20, no. 3, pp. 273–297, 1995.

[15] C.-C. Chang and C.-J. Lin, "LIBSVM: A library for support vector machines," *ACM Transactions on Intelligent Systems and Technology*, vol. 2, pp. 27:1–27:27, 2011.

[16] L. Breiman, "Random forests," *Machine learning*, vol. 45, no. 1, pp. 5–32, 2001.